Wind Energy

WILEY

RESEARCH ARTICLE OPEN ACCESS

A Safety-Aware Framework for Offshore Wind Turbine Maintenance

Anna Haensch[1] | Eleonora M. Tronci[2] | Aidan Banerjee[3] | Veronica Valencia[4] | Babak Moaveni[5]

[1]Data Science Institute, University of Wisconsin-Madison, Madison, Wisconsin, USA | [2]Department of Civil and Urban Engineering, Center for Urban Science and Progress, New York University, New York City, New York, USA | [3]Tufts Institute for Artificial Intelligence, Tufts University, Medford, Massachusetts, USA | [4]Department of Bioengineering, Northeastern University, Boston, Massachusetts, USA | [5]Department of Civil and Environmental Engineering, Tufts University, Medford, Massachusetts, USA

Correspondence: Eleonora M. Tronci (emt377@nyu.edu)

Received: 10 September 2024 | **Revised:** 24 July 2025 | **Accepted:** 24 September 2025

Funding: This study was supported by the National Science Foundation (2230630).

Keywords: economic modeling | maintenance | offshore wind | prospect theory | worker safety

ABSTRACT

In this paper, we suggest a framework for determining the best operation and maintenance strategies for offshore wind turbines. The framework takes into account both quantitative and qualitative data gathered from the wind turbines. The proposed framework consists of a simulation-optimization approach for designing, planning, and scheduling maintenance operations for offshore wind farms and finding the optimal intervention solution for minimizing costs while keeping a high availability of wind turbines and guaranteeing safety standards for workers. Several parameters and constraints are addressed to account for the realistic complexity of the problem, such as weather conditions, resource cost, and maintenance duration. A numerical case study focusing on offshore wind turbine blade maintenance is presented to demonstrate the implementation of the proposed framework. The example simulates realistic defect progression scenarios, stratified by severity level, and incorporates empirically grounded estimates of failure rates, repair costs, technician requirements, and vessel logistics. The study illustrates how the simulation-optimization approach integrates economic considerations, resource constraints, and safety risk factors to support data-informed maintenance scheduling decisions under uncertainty.

1 | Introduction

In March 2021, the United States set an ambitious goal to install 30 GW of offshore wind energy capacity on the outer continental shelf by 2030, signaling strong support for the industry's expansion [1]. Achieving these deployment goals will require a workforce that is sufficient in size and well-trained to meet the specific demands of offshore wind energy development. Ensuring safety remains a top priority for the offshore wind energy sector. Yet there is ongoing uncertainty about the specific safety standards and training requirements needed, as well as the roles various stakeholders will play in maintaining safety.

An effective and reliable maintenance strategy aims to maximize economic benefit, extend components' lifespans, reduce the number of emergency repairs, decrease overtime labor costs, and relieve the working stress and risk for the personnel involved [2]. Moreover, this must be done in a way that accounts for the stochastic attributes of uncertain maintenance outcomes and deviations between predicted and actual failure scenarios

Anna Haensch and Eleonora M. Tronci contributed equally to this work.

[3]. It is estimated that the operations and maintenance (O&M) contribute nearly 35% of the levelized cost of energy for a fixed-bottom offshore wind farm [4]. In this work, we propose a condition-based maintenance strategy that combines relevant information about an offshore wind turbine's (OWT's) current condition with statistical models of failure risk and external factors such as cost and worker safety.

The strategy proposed here is a multicriteria decision-making framework similar to those initially developed for formalizing and optimizing decisions for civil engineering systems [5, 6]. The framework consists of three phases (see Figure 1): in Phase I, the technical state of the OWT is assessed; in Phase II, a set of contingencies and outcomes is constructed (these are expressed in terms of economic and safety impact); and finally, in Phase III, a decision model is formulated, which assesses the value of all possible interventions, and appropriate action is chosen.

In contrast to previous work on maintenance decision frameworks, the strategy proposed here explicitly combines economic costs with worker safety, allowing for a multistakeholder optimization scheme. The novelty of this framework lies in its application of cumulative prospect theory (CPT) to offshore wind maintenance to account for varying risk tolerances among stakeholders, which is crucial in managing complex offshore environments. Furthermore, unlike existing frameworks that typically focus on economic costs or damage evaluations, this work integrates safety considerations directly alongside economic assessments to offer a holistic view of maintenance planning. These innovations contribute to a more resilient and adaptable maintenance strategy for the offshore wind sector, aligning with the ambitious goals of expanding wind energy capacity while prioritizing worker safety and operational efficiency.

In Section 4, a numerical example is presented, focusing on turbine blade defects using the cost evaluation provided for the 6.1-MW National Renewable Energy Laboratory (NREL) offshore reference project turbine as a case study [4]. This example demonstrates the application of the proposed framework by simulating the progression of defects within the turbine blade over time. Various stages of defect development are modeled, ranging from minor wear to severe damage requiring replacement, and potential maintenance strategies are assessed at each stage. Because access to real-world datasets involving offshore wind turbine failures, repair events, or safety incidents is extremely limited due to proprietary restrictions and the sensitive nature of O&M logistics, we employ synthetic data. These data are calibrated using publicly reported statistics on failure rates, downtime costs, repair durations, and vessel logistics. The example illustrates how the proposed decision-making framework integrates defect detection, economic modeling, and safety risk assessment in a realistic offshore operational context. This case study illustrates how the framework integrates defect detection, economic impact analysis, and safety considerations to guide optimal maintenance decisions, highlighting its relevance in real-world offshore wind turbine operations.

2 | Background

2.1 | Decision Frameworks

This paper presents a decision framework that involves multiple decision-makers and varying scales of safety and economic risk. In behavioral economics, decisions under risk are often modeled using cumulative prospect theory as introduced by Tversky and Kahneman [7]. The CPT model balances the risk of extreme events with the more average (i.e., likely) events and calibrates risk according to a neutral reference point. Significantly, this allows a CPT model to incorporate the cognitive and emotional processes of decision-making under uncertainty by weighting outcomes against this reference point. This type of modeling is particularly useful for scenarios where multiple stakeholders have differing neutral reference points.

Many empirical studies have been done to connect the CPT model to real-world decision-making in nautical navigation [8], wind energy procurement [9], and disaster response [10]. The concept of CPT has also been used to develop broad maintenance decision frameworks for engineered systems [11–13]. The present work builds on these prior investigations to develop a safety-aware decision framework that focuses on the maintenance objectives of the offshore wind sector. Unlike in prior work, the work ties human risk directly to the labor involved in the maintenance of the system rather than the human risk inherent in the failure of the system.

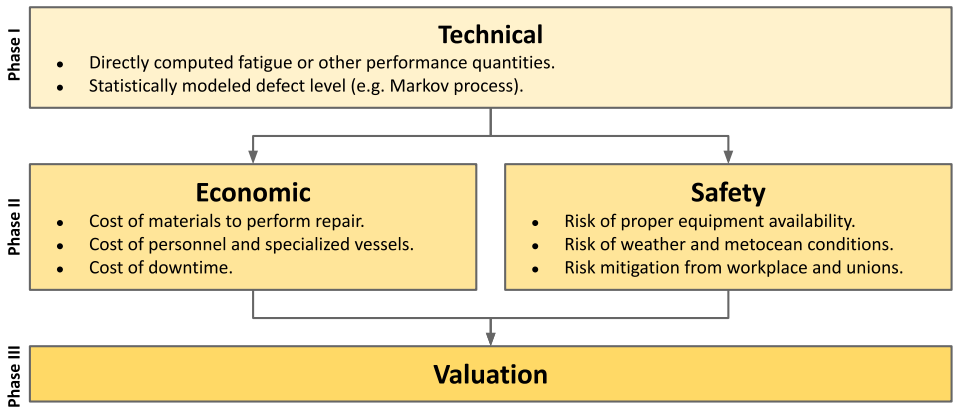

FIGURE 1 | The multifactor decision model combines a technical fatigue and defect assessment to learn the state of the equipment (Phase I), followed by a set of contingencies and outcomes based on economic and safety considerations (Phase II), and finally, a formal valuation of the decision space to arrive at an optimal course of action (Phase III).

2.2 | Maintenance Strategies

The proposed framework is applied within the context of offshore wind maintenance due to the unique operational and environmental challenges that offshore environments present. Offshore wind turbines face harsher weather conditions and accessibility issues, creating heightened safety risks and driving up maintenance costs. These factors necessitate a maintenance strategy that accounts for both economic considerations and safety risk perception, especially under uncertain environmental conditions.

Maintenance consists of activities to ensure that a WT is in working order and fulfilling its functions [14]. This typically involves deploying a technical crew on a transfer vessel to visit the turbine and perform required or scheduled maintenance. Activities related to offshore WT maintenance can be divided into preventative and condition-based. Although preventative maintenance involves periodically servicing the WT according to a fixed maintenance schedule, condition-based maintenance actions are only carried out in response to updated WT condition status [15]. As such, there are some explicit trade-offs between availability and reliability, depending on the choice of maintenance strategy, and some of this is borne out in the overall maintenance costs [16]. This work assumes a condition-based maintenance strategy, expanding upon its traditional framework. Traditional condition–based maintenance model frameworks incorporate variables related to component reliability, such as mean time to failure [17] or remaining useful life [18]. These quantities can be approximated by component-level annual failure rates [19], comprehensive fatigue life estimates [20], or latent state modeling techniques [21, 22].

In decision models related to maintenance, it is often important to consider the many stakeholders involved in decision-making, such as developers, technicians, vessel operators, and other onshore support [23, 24]. These models commonly take an economic cost and benefit approach [25], incorporating levelized cost of energy [26], WT availability [27], and fluctuating market conditions [28]. All of these models incorporate a degree of uncertainty around damage modeling, risk assessment, and maintenance outcomes [3, 29], but they often lack a fully integrated approach that considers additional decision-driving factors.

2.3 | Probabilistic Defect Assessment

Failures in WTs can be categorized into two main sources: (1) long-term operation and aging and (2) short-term overload and sudden breakdown. The likelihood of short-term failure is often higher in the first 1–3 years of operation, whereas long-term aging failures often occur within the last few predicted operational years. In engineered systems, this type of survival behavior is commonly modeled with a Weibull distribution to determine a probabilistic estimate of time to failure [30].

The types of failures experienced by a WT can be categorized by severity and overall turbine health. For component-based failures, we consider the three common failure classifications as in recent work (see, e.g., [31–33]): minor repair, major repair, and major replacement. Minor repairs include operational errors, electrical component malfunctions, and any hindrance to operation that can be fixed within 30 hours. Major repairs are more often related to intense structural damage and damaged or broken components and often take 30–120 h to complete. Major replacements are often connected to complete component failure and require an overhaul of the component, often taking over 120 h to complete. The probability of minor repairs versus major repairs varies between components, but on average, minor repairs occur six times more frequently than major repairs [31].

2.4 | Maintenance and Repair Costs

The overall maintenance costs can be broken down into fixed and variable costs. Fixed costs include material costs associated with carrying out routine maintenance or defect repair [34]. These costs vary significantly by component and defect severity [31].

Variable costs include factors related to transportation, logistics, personnel, and downtime, which scale with the amount of time it takes to complete a maintenance action. Depending on the turbine's size and the defect's severity (Table 1), it might be necessary to charter specialized crew transport vessels, heavy-lifting vessels, or even helicopters. These can vary in price and typically incur daily use costs as reported in [35] and shown here in Table 2. Variable costs include personnel costs to operate the vessels and a team of specialized technicians to perform the repair [31, 36].

TABLE 1 | Estimated vessel requirements by defect type, as reported in [35].

Category	Description
Minor repairs	Can be completed by a single crew transfer vessel (CTV) or a helicopter.
Major repairs	Requires a crew transfer vessel (CTV) and/or a service operation vessel (SOV), depending on how many workers are needed to make repairs.
Major replacement	Requires a service operation vessel (SOV) or heavy lifting vessel (HLV) for large components, which is extremely costly because of low supply of these vessels.

TABLE 2 | Estimated vessel costs by type, as reported in [35].

Vessel type	Vessel cost/day
Heavy lifting vessel (HLV)	$220,000.00
Service operation vessel (SOV)	$38,421.90
Crew transfer vessel (CTV)	$2561.46
Helicopter	$701.77
Unmanned aerial vehicle (UAV)	$300–$500
Jackup boat	—

Additionally, costs related to turbine downtime scale with the amount of time that the turbine is not operational. Downtime consists of the duration of time that the turbine is not operating as intended. This includes how much time technicians spend to carry out the repair (sometimes called the "mean time to repair" or MTTR) [37]. The duration of the repair time varies by component and defect severity, but extensive surveys out of the European wind industry give component-wise estimates of repair times [19, 31]. Costs per hour of downtime are subject to the particulars of a power purchase agreement and the changing price of energy, but most current US wind power purchase agreements have a purchase price of less than 2 cents per kWh [38]. Downtime costs become especially relevant in the long term when considering the levelized cost of energy for offshore wind [32].

2.5 | Safety Analysis

Prioritizing worker safety is crucial in developing a multifactor decision framework for offshore wind turbines. Insights and concerns from other industries, such as onshore wind, oil and gas, civil construction, and other countries, highlight the importance of having a robust and established set of guidelines in place [39]. In the context of offshore wind energy, Europe typically follows a prescriptive regulatory approach with detailed guidelines and significant government involvement in planning and development [40]. In contrast, the United States employs performance-based regulatory regulations that specify desired safety and environmental outcomes without dictating specific methods, allowing flexibility for regulated entities in choosing the best methods to meet their goals [41].

A hierarchy of safety standards (described in Figure 2) quantifies safety in offshore wind operations, providing a structured approach and incorporating various levels of regulatory and operational guidelines [41]. At the top of the safety hierarchy for offshore wind turbines is the Federal Regulatory Authority, which includes the Bureau of Safety and Environmental Enforcement (BSEE) and the Bureau of Ocean Energy Management (BOEM), which together handle the Department of the Interior's offshore renewable energy regulations, detailed in the 2024 Code of Federal Regulations 30 CFR part §585–586 (BOEM) [42] and 30 CFR part §285 (BSEE) [43]. Key documents reviewed by BSEE and submitted to BOEM include the Site Assessment Plan (SAP), Construction and Operations Plan (COP), and General Activities Plan (GAP). The SAP details site assessment methodologies; the COP outlines construction, operation, and decommissioning processes; and the GAP covers smaller-scale activities. These documents ensure compliance with federal regulations and incorporate safety measures such as a Safety Management System (SMS) or Emergency Response Procedures. BSEE ensures the safe and environmentally responsible design, fabrication, installation, operation, and decommissioning of offshore wind energy facilities, enforcing compliance with all relevant safety, environmental, and conservation laws and regulations from construction through decommissioning [44]. BOEM oversees prelease activities and approves COP terms, with BSEE helping to develop COP terms and conditions to ensure comprehensive workplace safety.

BSEE and BOEM set outcome-based goals, allowing operators to adopt the latest technologies and practices. This encourages innovation and market-driven development, emphasizing risk management through SMS and other documentation. This flexible approach helps the US offshore wind industry maintain rigorous safety and environmental standards. However, the industry and developers must still demonstrate to BSEE that they have identified relevant risks and implemented appropriate controls. This approach promotes innovation and adaptability while ensuring compliance with safety and environmental standards.

Below the federal requirements is the SMS framework, which encourages operators to seek certification through recognized standards. These certifications include ISO 45001, familiar to European offshore wind operators; API RP75W, used by US offshore oil and gas operators; ANSI/AHA Z10, known among manufacturers and fabricators; and the ISM Code, specific to vessel operations. Achieving certification under these standards ensures that the SMS framework meets international best practices for safety management.

A Safety Management System is a set of interrelated or interacting elements of an organization to establish policies, objectives,

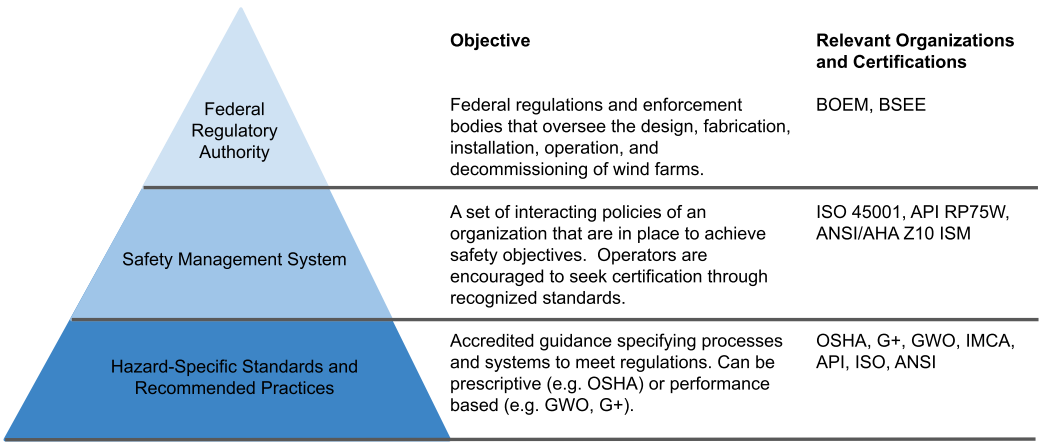

FIGURE 2 | A hierarchy of safety standards exists to ensure that operators have the appropriate knowledge, systems, and processes in place to meet safety and environmental regulations.

and processes to achieve safety objectives. An example subset consists of the Emergency Response Procedures (ERP), which are plans prepared to respond to emergencies, including both onshore and offshore actions and support, to mitigate safety and environmental consequences. An SMS has the aim of managing risks associated with various activities: leadership and contractor management, hazard identification and risk assessment, risk controls and planning, workforce engagement, evaluation and improvement, emergency response plans, regulatory requirements (including remote monitoring and control), and use of standards. Developers submit their SMSs to BOEM as part of their COP, which can be approved, disapproved, or approved with modifications. BSEE would receive and review the SMSs and develop terms and conditions for BOEM's COP relevant to BSEE jurisdiction.

At the base of the hierarchy are the Hazard-Specific Standards and Recommended Practices (RP), which provide accredited guidance specifying processes and systems to meet regulations and that can be either prescriptive, like OSHA standards [45], providing clear regulations that must be followed, or performance-based like those from the Global Wind Organisation (GWO) offering flexibility in achieving safety outcomes [46]. The GWO has developed training standards for the offshore wind industry with the goal of making H&S training standardized across the industry to raise standards and to make it easier for companies to ensure their employees have been adequately and uniformly trained. The GWO has developed standards that cover training in areas including basic safety, advanced rescue, and first aid [47].

Hazard-specific recommended practices are often provided by industry safety organizations such as G+ Global Offshore Wind Health and Safety Organisation, which releases an annual report on safety incidents and good practice guidance for the industry, or the International Marine Contractors Association (IMCA), which produces industry guidance and best practices for vessel operations, dynamic positioning, ROV, lifting, marine operations, and training. These are largely performance-based and tailored to address particular risks in offshore wind operations [48, 49].

In US offshore wind energy, several RPs from other offshore industries are used, though none are specific to this sector. These RPs are created by standards bodies like the American Petroleum Institute (API), International Standards Organization (ISO), and American National Standards Institute (ANSI) in collaboration with industry organizations such as the American Clean Power Association to develop consensus by convening industry stakeholders. Developers can choose the most suitable RP for their project and must prove safety through performance-based audits. These standards enhance worker safety by clarifying training requirements for developers, subcontractors, and regulators.

3 | Methodology

The following section combines the abovementioned cost and safety discussion into a comprehensive quantitative decision model. Following the conventions of cumulative prospect theory (CPT), the decision model will be framed in terms of events (i.e., different types of interventions), outcomes (i.e., economic costs and safety risks), and the associated likelihoods, risks, and rewards of each [7]. Unlike classical economic utility theory, CPT allows decision makers to explore a large space of possibly competing events and outcomes, where the risks are calibrated relative to a decision maker's reference point (see, e.g., [50, 51]).

Suppose the space of possible interventions, ordered by complexity, is given by

$$I = \{I_0, \ \dots, I_m, \ \dots, I_M\}$$

(see Table 3), and suppose that all possible real-valued outcomes are sorted from worst to best relative to a neutral reference point, $x_0 \in \mathbb{R}$, where $x < x_0$ are considered to be losses and $x > x_0$ are considered to be gains. The prospect value, P_m, for an intervention, I_m, is evaluated in terms of the possible outcomes, and their associated probabilities given by $p(x_{im}) = p_{im}$.

$$X_m = \{x_{-\ell m}, \ \dots, x_{-1m}, x_{0m}, x_{1m}, \ \dots, x_{km}\},$$

For simplicity, the m subscript is dropped in the following discussion. The value is placed on the outcomes in X by applying a strictly increasing utility function, $v(x): X \to \mathbb{R}$ with $v(x_0) = 0$. The prospect value for an intervention in I can then be written as

$$P = \sum_{i=-\ell}^{-1} \pi_i^- \cdot v(x_i) + \sum_{i=0}^{k} \pi_i^+ \cdot v(x_i), \tag{1}$$

where π_i^- and π_i^+ are the decision weights that adjust the marginal contribution of outcome x_i to the overall value of the prospect. These are computed in terms of the outcome probabilities and a probability weighting function, w. In this way, weighted marginal probabilities are obtained as

$$\pi_k^+ = w(p_k) \ \text{ and } \ \pi_i^+ = w(p_i + \dots + p_k) - w(p_{i+1} + \dots + p_k) \tag{2}$$

for $0 \le i \le k-1$ and

$$\pi_{-\ell}^- = w(p_{-\ell}) \ \text{ and } \ \pi_i^- = w(p_{-\ell} + \dots + p_i) - w(p_{-\ell} + \dots + p_{i-1}) \tag{3}$$

for $1 - \ell \le i \le 0$. A probability weighting function aims to allow utility theory to match common sense by systematically enlarging ratios between high probability events by choosing a

TABLE 3 | Each of the M possible interventions has a set of possible outcomes with an associated economic prospect and safety prospect. The economic and safety prospects are formulated as in Equation (6).

Intervention	Outcome	Prospect
I_0	$X_0 = \{x_{-\ell 0}, \ \dots, x_{-10}, x_{00}, x_{10}, \ \dots, x_{k0}\}$	P_0
⋮	⋮	⋮
I_m	$X_m = \{x_{-\ell m}, \ \dots, x_{-1m}, x_{0m}, x_{1m}, \ \dots, x_{km}\}$	P_m
⋮	⋮	⋮
I_M	$X_M = \{x_{-\ell M}, \ \dots, x_{-1M}, x_{0M}, x_{1M}, \ \dots, x_{kM}\}$	P_M

weighting function that overweights low values and underweights high values, leading to a regressive effect (utility theory is subject to the so-called "common ratio effect," which observes that the common sense choice often differs from the best choice under utility theory; for example, people often opt for a marginally higher payoff with marginally higher risk when an event is very rare to begin with—e.g., lottery tickets—but, at the same time, will opt for a marginally lower payoff when the choice is between a guaranteed success and a 50–50 chance of success [52]).

One good choice for this function is described by Prelec [53] and given by

$$w(p) = e^{-(-\ln(p))^{\gamma}} \tag{4}$$

for $p \in (0,1]$ and $w(0) = 0$, where $0 < \gamma \leq 1$. One typical utility function associated with this choice of probability weighting is the power utility function (see, e.g., [50, 54–56]). Therefore, the prospect is completely parameterized by the set ϕ, which includes x_0, γ, and any other parameters of the utility function, and the prospect value of an intervention is given by

$$P(\phi) = \sum_{i=-\ell}^{-1} \pi_i^- \cdot \left[(x_i - x_0)^{\alpha^+} \right] + \sum_{i=0}^{k} \pi_i^+ \cdot \left[-\beta\left(-(x_i - x_0)\right)^{\alpha^-} \right], \tag{5}$$

where π_i^+ and π_i^- are as in Equations (2) and (3).

In the context of the present problem, outcomes of an intervention I_m are considered in terms of economic prospects, V_m, and safety prospects, R_m (see Table 3). For each of these, a prospect value can be computed as

$$P_m(\phi_{\text{economic}}) = \sum_{i=-\ell_m}^{k_m} \pi_i \cdot v(x_i) \text{ and } P_m(\phi_{\text{safety}}) = \sum_{i=-\ell_m}^{k_m} \pi_i \cdot u(x_i), \tag{6}$$

where v is an economic utility function and u is a safety utility function, whereas ϕ_{economic} and ϕ_{safety} and are the set of parameters used to parameterize the two utility functions. They include quantities such as utility shaping parameters or reference neutral points, or also decision weights. The utility functions and the parametrizing characteristics will be described more fully in the following section.

3.1 | Defect Level Inference

Suppose a defect state, d_0, is entered at time t_0 and is detected at time t_n. Assuming that time is measured in days, this means n days have passed between the time the defect state was entered and the time the defect was detected. We will consider a set of three possible defect levels: minor repair (1), major repair (2), and major repair with replacement (3).

Based on the defect level and time since detection, the goal is to choose the best possible intervention out of the set of possible interventions, $I = \{I_0, \ldots, I_M\}$, where intervention I_m corresponds to initiating repair on day t_{n+m}, that is, m days after the defect is detected. This intervention has a set of possible outcomes given by

$$X_m = \{x_{3m}, x_{2m}, x_{1m}, x_{0m}\}, \tag{7}$$

where x_{km} corresponds to entering defect level k on day t_{n+m} (defect level 0 corresponds to no defect). Note that these outcomes are ordered by descending index in order to sort from worst to best outcome, to keep in line with the conventions of cumulative prospect theory. At the time that the repair begins, the defect level is d_{n+m}, and when the repair is complete, the defect level is 0. A visual timeline of this process is shown in Figure 3.

In the time between the initial occurrence of the defect at time t_0, its detection at time t_n, and the initiation of repair at time t_{n+m}, we allow for a worsening of the defect, that is, $0 < d_0 \leq d_n \leq d_{n+m}$. The progression of defect levels in a turbine component is modeled as a Markov process. Markov models are particularly effective for systems where transitions between discrete states occur probabilistically over time, and the future state depends solely on the current state, a property known as the Markov property. The application of Markov models in reliability engineering is well established [57]. They have been effectively used to assess the reliability of repairable systems and to model the degradation processes of components subject to stochastic failures. For instance, studies have demonstrated the efficacy of Markov models in predicting the reliability of offshore wind energy systems and in modeling the degradation of wind turbines [58, 59]. Figure 4 illustrates the Markov chain model representing the probabilistic progression of defect states in an offshore wind turbine component over time.

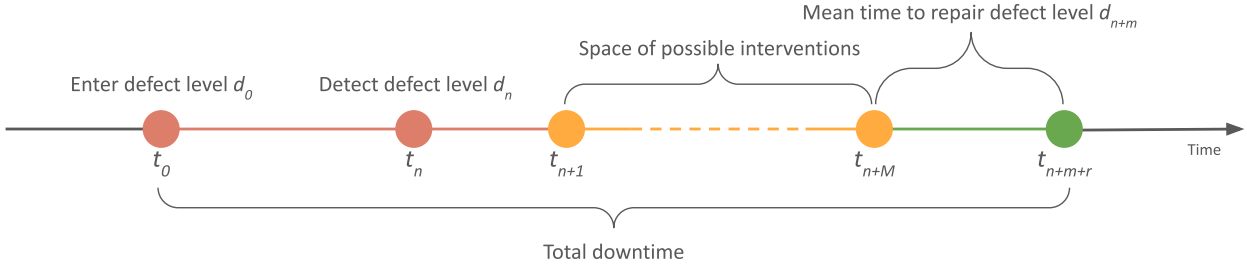

FIGURE 3 | The timeline for decision-making begins at time t_0 when the turbine enters defect level $d_0 > 0$. This defect is detected at time t_n, after which the space of possible interventions follows. The defect can continue to worsen during this time. After the repair is made, the defect level returns to 0 (i.e., operational) at time t_{n+m+r}.

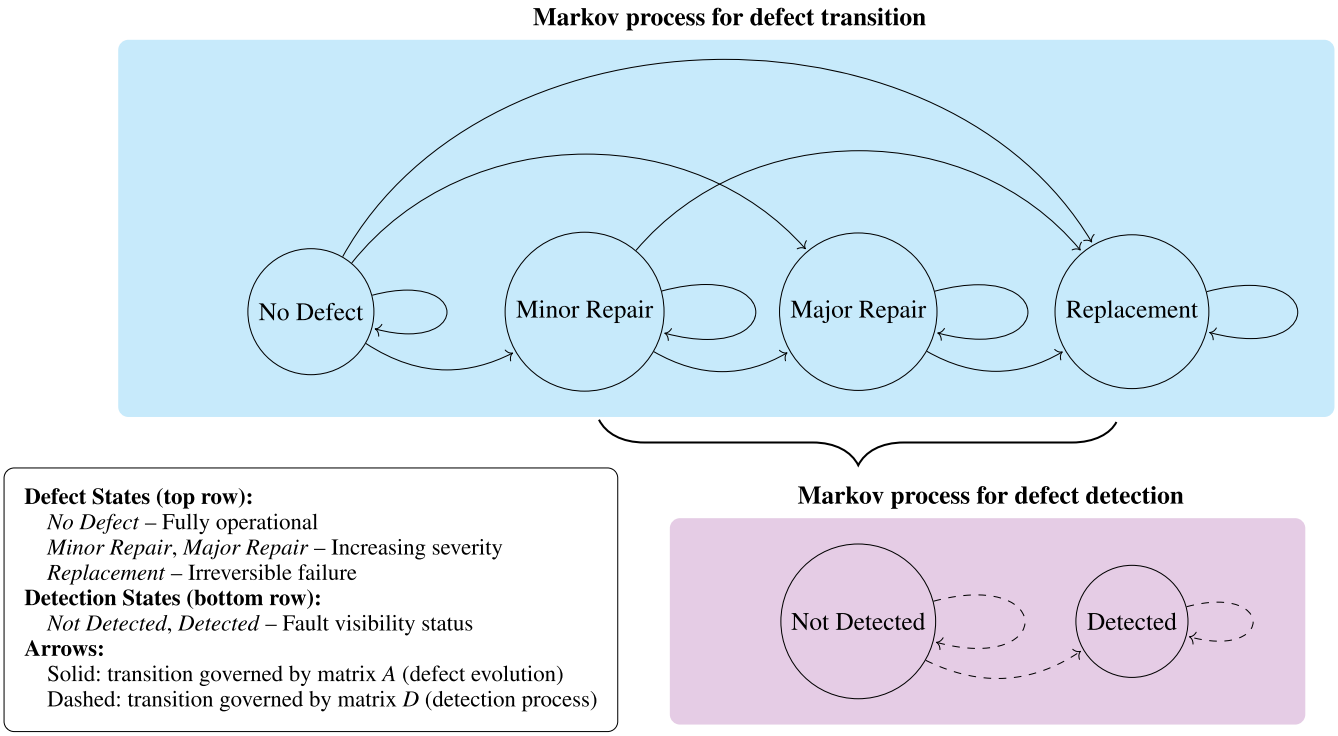

FIGURE 4 | This directed graphical model illustrates the underlying Markov processes involved in defect accumulation and defect detection. The top row of the graphical model shows the transitions between operational and defect states with probabilities associated with the test case described in Section 4. Solid arrows indicate a transition with an associated probability; the base of the arrow is the state at time t, and the head of the arrow is at time $t+1$. Once a repair or replacement state is entered, a second Markov model is activated. This is shown in the bottom row, where arrows indicate a transition from "not detected" to "detected" with associated probabilities.

The top row of circles depicts potential defect states, ranging from "no defect" and "replacement," with intermediate states such as "minor repair" and "major repair," indicating increasing severity and repair requirements. The arrows between states represent possible transitions, each governed by a probability that reflects the observed behavior of defects in turbine components.

The bottom row shows a parallel Markov process for the detection status of defects, transitioning between "not detected" and "detected" states. Detection status is critical in maintenance decision-making, as defects that go undetected may worsen and require more extensive interventions. The dashed lines illustrate that defect detection progresses concurrently with the defect's severity, influencing the likelihood and timing of repair actions.

Modeling these transitions mathematically requires knowledge of the current system state and the probability of entering one of the more severe defect states. This information is expressed as a 4×4 Markov transition matrix, A, where the ij^{th} entry is the probability of transitioning from defect level i to defect level j, which is represented in Figure 4 by the arrows. Note that A is an upper triangular matrix because a defect will only get worse without intervention. Let $\mathbf{e}_{d_n}$ be the row vector, which is 1 in position d_n and 0 elsewhere. Then, the probability of experiencing outcome x_{km} (i.e., entering the k^{th} defect level at time t_{n+m}) is given by

$$p_{km} = \left(\mathbf{e}_{d_n} A^{n+m}\right)_k. \tag{8}$$

In a similar manner, whether or not a defect has been detected will also be modeled as a Markov process, where D is the 2×2 upper triangular matrix with the transition probabilities between "not detected" and "detected."

3.2 | Economic Cost Model

We will estimate the utility of intervention I_m as the cost to repair m days after a defect is detected. At this point, the defect level is $d>0$, and t days have passed since the defect occurred. The cost to repair is a function of the defect level and the number of days elapsed, and it is given by

$$c(d,t) = f(d)\cdot\left[c_{vessel}(d) + c_{person}(d)\right] + (f(d)+t)\cdot c_{down} + c_{materials}(d), \tag{9}$$

where $f(d)$ is the mean time to repair a defect of level d, $c_{vessel}(d)$ and $c_{person}(d)$ are the associated vessel rental and personnel costs per day for a defect of level d, $c_{material}(d)$ is the material cost to repair a defect of level d, and the constant value c_{down} is the cost per day for turbine downtime. Tying this back into the framework of cumulative prospect theory, we define the economic utility of outcome x_{km} of intervention I_m as $v(x_{km}) = c(k, n+m)$.

3.3 | Risk Assessment and Safety Cost Model

The safety component of the decision-framework model is broken down into a risk score and a safety cost model. This distinction is functional in dividing between factors that affect the risk score and those that are affected, providing key

insights into understanding the dynamics of safety management in offshore wind operations. The risk score is designed to account for and integrate key safety factors, like delay, weather, and equipment suitability, which directly impact the risk score because they influence the likelihood and severity of potential incidents. This comprehensive risk assessment enables identifying and quantifying hazards associated with offshore wind energy operations. In contrast, factors affected by the risk score, such as insurance costs and reputational impact, are consequences that result from the quantified risk [60]. Higher risk scores typically lead to increased insurance premiums because insurers perceive a greater likelihood of claims. Reputational impacts can arise from high-risk incidents, damaging the credibility and market position of the operator. Therefore, the safety cost model acts as a bridge, translating the inherent hazards of offshore operations captured by the risk score into financial and operational repercussions, highlighting the importance of mitigating primary risk factors to control subsequent costs and impacts.

In offshore wind energy operations, workers' safety conditions are addressed and planned for by developers in the design of safety management systems that are often translated into a risk assessment matrix (RAM) to evaluate safety operations systematically. The matrix assesses potential hazards by categorizing the severity and likelihood of incidents, thereby guiding decision-making and risk mitigation strategies. Severity levels range across different injury concerns from no injury to multiple fatalities, whereas likelihood levels range from highly unlikely to highly probable. These levels are determined by factors such as equipment availability, weather conditions, and time delays. The risk score is calculated as the product of severity and likelihood, and it integrates the impact and probability of an event, providing a comprehensive measure of risk.

Figure 5 shows an example of a customized risk assessment matrix below that is tailored specifically for offshore wind operations. This matrix will be later used in the numerical application. It incorporates severity and likelihood scales relevant to the specific hazards encountered during these operations, such as severe weather conditions, equipment failure, and personnel safety issues. The matrix consists of categories ranging from A1 (*highly unlikely*, *no injury*) to E5 (*highly likely*, *multi-fatalities*), each associated with a risk score using a three-color scheme: acid green (low risk, 0–0.5), peach (moderate risk, 0.5–1), and magenta (high risk, 1–1.5). Depending on the specific activity and weather conditions, such as wave height for vessel transfer and wind speed for working at height, scenarios are assessed and placed within this matrix. For instance, wave heights and wind speeds are mapped to their respective risk categories, determining the necessary safety measures. This approach integrates quantitative risk assessment into decision-making processes.

These risk assessment matrices are conditional upon the intervention type and phase of the intervention. In this setting, our intervention outcomes are still given by

$$X_m = \{x_{-\ell m}, \ \dots, x_{-1m}, x_{0m}, x_{1m}, \ \dots, x_{km}\},$$

but now, the x_{im} is an external or environmental state that might be encountered in the m^{th} intervention.

One of the key contributions of this work is proposing a decision-making framework that enables one to account for how risk is perceived differently by various parties involved in the decision-making process. These individuals, or "agents," have different preferences and levels of risk tolerance that inform their perceived risk. This subjective assessment translates into a modulation of the risk score defined and calculated from the risk assessment matrix, and it is modeled using a risk perception function, r_j defined for each party or agent involved, j. The risk perception function is a mathematical model that translates a quantitative measure of risk into a perceived level of risk. The design of the risk perception function can follow different strategies. A piecewise linear approach (see Figure 6) is one common choice because it captures a basic threshold effect, where risk perception is minimal below a threshold x_0 and increases linearly beyond it [61]. However, it lacks flexibility for modeling nonlinear escalation in perceived risk. To overcome this limitation, in this work, the authors propose a piecewise risk perception function r_j as presented in Equation (10) and shown in Figure 6,

$$r_j(x_{im}) = \begin{cases} \rho_j \cdot (x_{im} - x_0)^{\eta_j} + h & \text{if } x_{im} \geq x_0 \\ h & \text{if } x_{im} < x_0 \end{cases}, \tag{10}$$

Severity/ Likelihood	Highly Unlikely A	Unlikely B	Possible C	Likely D	Highly Likely E
No Injury: 1	A1	B1	C1	D1	E1
Minor:2	A2	B2	C2	D2	E2
Major:3	A3	B3	C3	D3	E3
Fatalities:4	A4	B4	C4	D4	E4
Multi-Fatalities:5	A5	B5	C5	D5	E5

Severity		Likelihood	
1	No Injury	A	Highly Unlikely
2	Minor Injury	B	Unlikely
3	Major Injury	C	Possible
4	Fatality	D	Likely
5	Multiple Fatalities	E	Highly Likely

FIGURE 5 | Risk assessment matrix.

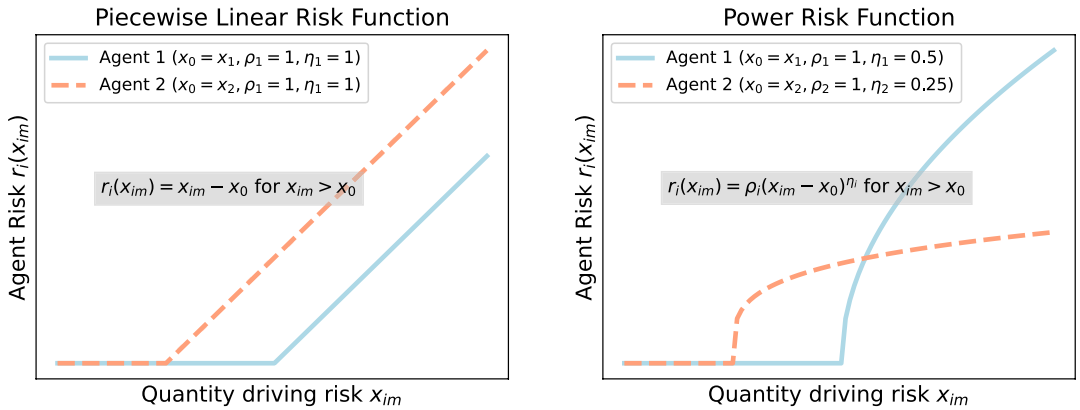

FIGURE 6 | Examples of risk perception function as described in Equation (10). The piecewise linear function on the left corresponds to $\rho_i = 1$ and $\eta_i = 1$ for both agents. The power function on the right corresponds to different positive values for η_i.

where ρ_j is a scaling factor that adjusts the intensity of the perceived risk for each agent; x_0 is the threshold beyond which risk starts to be perceived; and η_j determines the curvature of the function, allowing for different sensitivities to risk as x_{im} varies. It is possible to consider x_{im} as representative of one or the primary quantity driving the risk, such as wind speed when working at height or wave height when performing a vessel transfer operation. This work focuses on a single risk variable x_{im}, although this framework could be extended to a weighted sum or other aggregate function that includes multiple risk covariates.

This piecewise function effectively models risk perception, being able to account for a threshold x_0 below which risk perception is constant, assuming a small value (or 0). This aligns with the idea that risks below a certain level are somewhat small or not perceived as significant. The parameters η_j and ρ_j allow for flexibility in shaping the risk perception curve, accommodating various levels of sensitivity to risk. For instance, different agents can have different values for these parameters, reflecting their unique risk perceptions. Finally, the nonlinear nature of the function when $x_{im} \geq x_0$ models how risk perception can increase at an accelerating rate, which is often observed in real-world scenarios.

The safety cost model $u_j(x_{im})$ for the i^{th} outcome of the m^{th} intervention by the j^{th} agent includes insurance and reputational costs, which are functions of the perceived risk

$$S_{im} = \sigma_j \cdot r_j(x_{im}) \tag{11}$$

and

$$R_{im} = \lambda_j \cdot r_j(x_{im}), \tag{12}$$

where σ_j and λ_j represent parameters that scale the perceived risk to reflect the actual insurance premium and potential impact on the developer's reputation for the j^{th} agent. They vary based on the insurance provider's assessment of risk and the coverage required, as well as the organization's public image, industry presence, and stakeholder engagement. The combined safety cost model for agent j becomes

$$u_j(x_{im}) = S_{im} + R_{im} = (\sigma_j + \lambda_j) \cdot r_j(x_{im}), \tag{13}$$

depending on the specific safety ramifications of intervention I_m and the inherent risk of outcome x_{im}.

3.4 | Decision Model

Prior to computing the prospect value, the probabilities given in Equation (8) are adjusted using the Prelec function and weighted marginal probabilities as in Equations (3) and (4). Combining all of this, we have an overall prospect for intervention I_m for agent j, which is given by

$$P_{mj} = \alpha \cdot P_m(\phi_{economic}) + \beta \cdot P_{mj}(\phi_{safety}), \tag{14}$$

where α and β are two weighting parameters that can be adjusted based on targeted relative model contributions of economic factors and safety factors. Alternatively, α and β could be scaling factors to recalibrate the base orders of magnitude of the economic and safety contribution. This might depend on how the risk cost is evaluated. From here, the optimal maintenance intervention is given by

$$I = \underset{m}{\operatorname{argmin}}\, P_m, \tag{15}$$

the intervention with the lowest prospect value.

4 | Numerical Example

This section applies the previously outlined methodology to a case study focusing on the maintenance planning of wind turbine blades. Blades are critical structural components that operate under complex loading conditions and are continuously exposed to harsh environmental factors, making them susceptible to various damage mechanisms. Common defects include leading edge erosion, adhesive joint degradation, trailing edge failure, buckling, and damage from lightning strikes. These defects can significantly impact the structural integrity and aerodynamic performance of the blades, leading to reduced energy production and increased maintenance costs [62]. Leading edge erosion is particularly prevalent due to the continuous impact of rain, hail, and airborne particles, which degrade the blade's surface and aerodynamic profile over time.

Adhesive joint degradation and trailing edge failures often result from fatigue loading and manufacturing imperfections, leading to delamination and structural instability. Buckling can occur under extreme loading conditions, compromising the blade's load-bearing capacity. Lightning strikes, although less frequent, can cause severe damage, including delamination and material ablation, necessitating extensive repairs or complete blade replacement [63].

Understanding these failure modes is essential for developing effective maintenance strategies. The subsequent analysis utilizes synthetic data calibrated with empirical statistics to model the progression of blade defects and evaluate the economic implications of different maintenance decisions. This approach enables the assessment of risk-informed maintenance planning, optimizing the balance between operational reliability and maintenance costs.

4.1 | Defect Severity Modeling and Cost Assessment for Wind Turbine Blade Maintenance

There are several downsides related to the development of damage in blades. Blade defects significantly impact the operational efficiency and financial performance of offshore wind farms. Leading edge erosion, for instance, can reduce aerodynamic efficiency, leading to a decrease in power output by up to 5% annually [64, 65]. Structural defects such as cracks and delamination compromise the integrity of the blade materials, posing risks of catastrophic failure if not promptly addressed. These defects often necessitate immediate maintenance actions, leading to turbine downtime. The duration of such downtime can vary from a few days to several weeks, influenced by the severity of the defect and the availability of repair resources. Extended downtime not only results in lost energy production but also incurs substantial maintenance costs, thereby impacting the overall economic viability of wind farm operations.

Given the critical role played by these structural components in the maintenance strategies for offshore wind farms, the following section focuses on this particular turbine component. To implement the proposed methodology, we utilize the NREL 6.1-MW offshore reference turbine as the basis for our case study. This turbine model is part of NREL's fixed-bottom offshore wind reference project, which is widely recognized in the industry for its comprehensive and publicly available data. The reference project reports a net capacity factor of 48.7%, reflecting realistic operational performance for offshore wind turbines in suitable wind resource areas.

For economic modeling, we assume a power purchase agreement (PPA) price of \$0.02 per kilowatt-hour (kWh), consistent with industry benchmarks for offshore wind energy [38]. Based on these parameters, the estimated cost of downtime per hour for the turbine is calculated as follows:

$$6{,}100\ \text{kW} \times \$.02\,/\,\text{kWh} \times 48.7\,\% = \$59.41.$$

Additionally, maintenance labor costs are incorporated into the economic analysis. According to the US Bureau of Labor Statistics, the median hourly wage for wind turbine service technicians was \$29.70 as of May 2023 [36]. This wage rate is used to estimate the labor component of maintenance and repair activities.

By employing the NREL 6.1-MW offshore reference turbine, we ensure that our case study is grounded in a well-documented and industry-accepted framework, facilitating the applicability and scalability of our findings to real-world offshore wind operations.

Wind turbine blade maintenance activities are systematically categorized based on the severity and nature of the damage, which directly influence the required repair strategies and associated resources. This classification is essential for optimizing maintenance operations and ensuring the structural integrity and performance of wind turbines.

Minor repairs [66] address superficial damages that do not compromise the blade's structural integrity but may affect aerodynamic performance. Common issues include leading-edge erosion, surface roughness, and minor coating degradation. Such damages are typically addressed through surface treatments like sanding and recoating, application of protective tapes, or minor patch repairs. These repairs are often conducted during scheduled maintenance intervals without necessitating turbine shutdown. Major repairs involve more substantial damage, such as nonstructural material matrix cracks or delamination. Repair techniques often include filling, sealing, and resin injections to restore structural integrity. These repairs often necessitate turbine downtime and may require specialized equipment and skilled personnel [67]. Finally, major replacements [68] encompass severe damage scenarios, such as total blade collapse resulting from delamination or buckling. The most common cause of major replacements in blades is lightning strikes, which can sometimes require the replacement of all three blades [69, 70].

This structured classification facilitates a risk-based approach to maintenance, allowing operators to prioritize repairs, allocate resources efficiently, and minimize turbine downtime. By understanding the severity and implications of different damage types, maintenance strategies can be tailored to ensure the longevity and optimal performance of wind turbine blades. Empirical data from Carroll et al. [31] provide detailed insights into the resource requirements associated with different repair categories. For instance, minor repairs, such as addressing leading-edge erosion, typically involve an average repair time of 9 h and require a small team of technicians. In contrast, major repairs, addressing more significant structural issues, demand longer repair times and larger teams. Major replacements, often necessitated by catastrophic failures like lightning strikes, involve extensive repair durations and substantial resource allocation. These metrics are crucial for modeling operational expenditures and are detailed in Table 4.

In the context of wind turbine blades, defects typically progress through identifiable stages, such as minor damage (e.g., surface erosion), moderate damage (e.g., delamination), and severe damage (e.g., structural failure). These stages can be represented as discrete states within a Markov model, with transition probabilities informed by empirical failure rates, such as those reported by Carroll et al. [31]. This study reports annual failure rates per turbine of 0.456 for minor repairs, 0.010 for major repairs, and 0.001 for major replacements. These rates are derived from extensive operational data,

making them a reliable foundation for our analysis. Using these failure rates, we construct a discrete-time Markov transition matrix, denoted as A, where the ij^{th} entry of A represents the probability of transitioning from the defect state i to state j within a given time interval:

$$p_{ij} \coloneqq p\left(d_t = j \mid d_{t-1} = i\right),$$

where d_t is the defect level at time t and t is measured in days.

This modeling approach allows for the quantification of the likelihood of progression from one damage state to another over a specified time horizon and enables the evaluation of the impact of different maintenance strategies.

To model the stochastic progression of blade defects, we define a row-stochastic transition probability matrix where each entry represents the probability of transitioning from defect level i to j in one time step (day). The matrix structure assumes monotonic deterioration, such that defects can only worsen or persist in the absence of repair:

$$A = \begin{bmatrix} 1-(p_{01}+p_{02}+p_{03}) & p_{01} & p_{02} & p_{03} \\ 0 & 1-(p_{12}+p_{13}) & p_{12} & p_{13} \\ 0 & 0 & 1-p_{23} & p_{23} \\ 0 & 0 & 0 & 1 \end{bmatrix}.$$

TABLE 4 | Average repair values associated with blade defects and failures as reported in [31]. Currency values are converted from Euros to USD using the historical 2016 average 1.11 Euro–USD exchange rate.

	Minor repair	Major repair	Major replacement
Material repair cost (USD)	189	1665	99,900
Number of technicians	2.1	3.3	21
Time to repair (hours)	9	21	288

From [31], we know that turbine blades have a 0.456 annual failure rate, which means the probability of requiring a minor repair in a given year is

$$1 - e^{-0.456} = 0.366.$$

Assuming the turbine begins in a fully operational state $x_0 = (1,0,0,0)$ (i.e., operational at time $t = 0$), its state after t days is given by the vector $x_0 A^t$. Therefore, after 365 days, we would expect

$$\left(x_0 A^{365}\right)_1 \approx 0.366.$$

To calibrate the transition probabilities, p_{ij}, we formulate an optimization problem that minimizes the squared difference between the expected number of failures $\hat{N}_k$ and the observed number N_k for each category k. Specifically, we solve

$$f = \min_{(p_{01},p_{12},p_{13})} \sum_k \left(N_k - \hat{N}_k\right)^2,$$

where

$$\hat{N}_k = \left(x_0 A^{365}\right)_k \cdot N_{\text{total}}.$$

This is achieved by using ordinary least squares minimization implemented using Scipy's `minimize` function with constrained optimization by linear approximation ("COBYLA"). The calibrated transition matrix obtained is

$$A = \begin{bmatrix} 0.945 & 0.053 & 0.001 & 0.000 \\ 0 & 0.997 & 0.001 & 0.001 \\ 0 & 0 & 0.999 & 0.001 \\ 0 & 0 & 0 & 1 \end{bmatrix}.$$

This matrix reflects realistic defect progression dynamics in turbine blades and is consistent with reported long-term reliability data, making it a valid and scientifically grounded choice for the defect modeling framework.

For numerical simplicity, we assume that $p_{02} = p_{12}$ and $p_{13} = p_{23}$, although this need not be the case. Figure 7 shows the sample economic prospect values for this numerical example. In all cases,

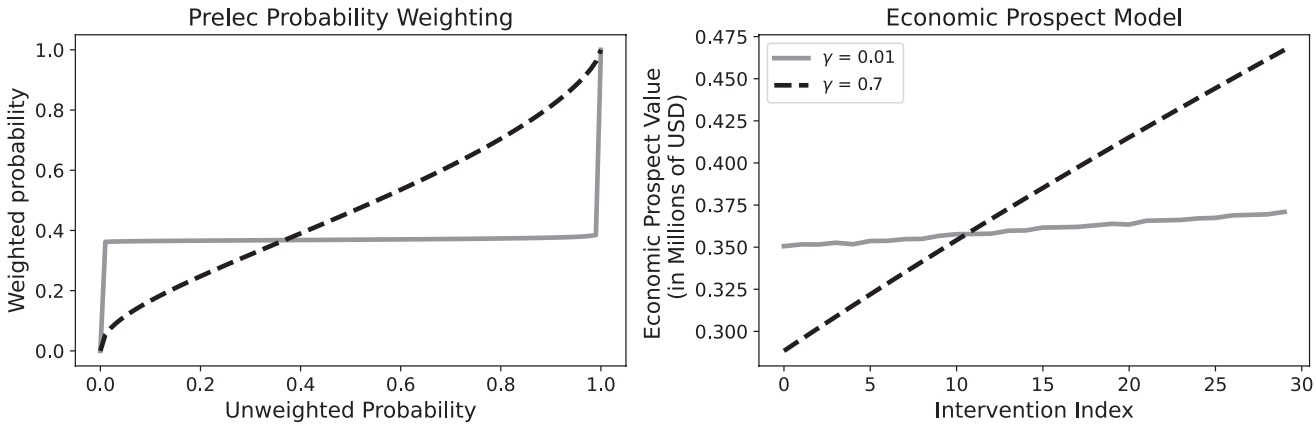

FIGURE 7 | Economic prospect values for varying interventions and choices for γ in Equation (4). The smaller values of γ correspond to giving roughly equal weight to all possible outcomes, whereas larger values stay closer to a linear probability weighting.

the economic prospect value increases over time since damage accumulates over time if left unchecked. The solid gray line in Figure 7 corresponds with $\gamma = 0.01$ in Equation (4), which gives nearly equal weight to all outcomes regardless of probability. Because probabilities of the outcomes evolve over time, and because the costs associated with each outcome differ, the gray light shows very slight instability. The black dashed line, on the other hand, corresponds to $\gamma = 0.7$, which always gives a strong priority to the most likely outcome, which, over time, becomes the most costly outcome. Notice that the two lines cross each other at intervention index 10, that is, intervention on the 10^{th} possible day.

Figure 8 illustrates the outcomes of using the Markov model described (Figure 4) in Section 3.1 combined with the described transition matrix to simulate defect, detection, and repair cycles for two turbines over 365 days. The x axis represents the days, whereas the y axis categorizes the type of defect or repair activity, ranging from "no defect" to "major replacement."

Turbine 1 (continuous gray line) experienced a total of 13 minor repairs, 0 major repairs, and 1 major replacement. The minor defects for Turbine 1 are frequent and spread throughout the year, indicating regular but less severe maintenance requirements. The major replacement is indicated by a significant spike near the middle of the year cycle, showing that this event required more resources and time. The flat area at the top of each spike represents the combined time between defect occurrence, detection, and repair (recall that there may be a lag between defect occurrence and detection).

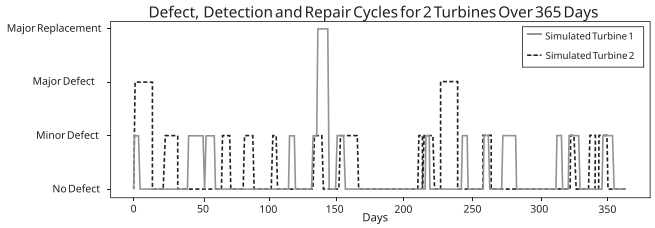

FIGURE 8 | Two simulated cycles of defect, detection, and repair. Turbine 1 required 13 minor repairs, 0 major repairs, and 1 major replacement. Turbine 2 required 13 minor repairs, 2 major repairs, and 0 major replacements.

Turbine 2 (dashed black line) required 13 minor repairs, 2 major repairs, and 0 major replacements. Similar to Turbine 1, Turbine 2's minor defects are distributed throughout the year, showing consistent, less critical maintenance. The two major repairs are noticeable on the graph as more intensive maintenance activities compared to the minor repairs.

Comparatively, both turbines underwent significant maintenance. The number of minor repairs is equivalent for Turbine 1 compared to Turbine 2, but Turbine 2 also needs major repairs, suggesting Turbine 2 might be slightly less reliable in terms of minor/major issues. Conversely, Turbine 1 experienced a major replacement, requiring the complete overhaul of a turbine component.

Figure 9 illustrates the proportion of turbines in different defect or repair states over time, specifically tracking 100 turbines across 365 days. The x axis represents the days, whereas the y axis indicates the proportion of turbines in each state. The green line represents turbines that are fully operational and have no defects. The yellow line shows turbines that are still operational but have some form of defect, either minor or major. These turbines continue to function despite the defect, but may require maintenance soon. The red line indicates turbines that are non-operational because they are undergoing repairs. This includes turbines in the more severe states of major repair or major replacement, where they are taken offline until the repairs or replacements are completed. The red line reflects the proportion of turbines out of service for active repair, whereas the yellow line covers those with defects that have not yet led to downtime.

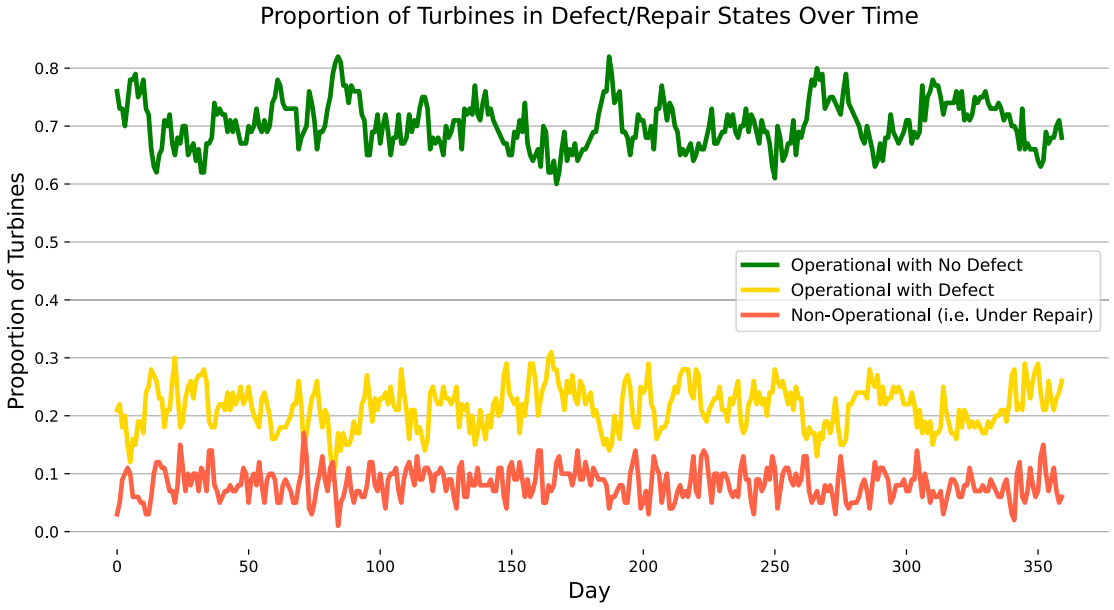

FIGURE 9 | Cycles of defect, detection, and repair were simulated for 100 turbines across 365 days. Overall, there is a defect-free fleet availability of around 70%.

Throughout the year, the proportion of defect-free operational turbines fluctuates but generally remains around 70%. This suggests that most turbines are kept in good working condition through regular maintenance and repairs. The operational turbines with defects, represented by the yellow line, show a consistent presence, indicating that although some turbines operate with minor issues, they are still functional.

The red line, representing nonoperational turbines under repair, remains steady at around 10% throughout the year. This proportion indicates that although the likelihood of turbines entering severe defect states, such as major repairs or replacements, is relatively low, the turbines that require these interventions remain out of service for extended periods. The transition matrix's final row, with a value of 1 in the "major replacement" state, indicates that once a turbine enters this state, it stays nonoperational until the repair or replacement is fully completed. This prolonged downtime, particularly for major repairs and replacements, leads to a consistent proportion of turbines being unavailable at any given time. The 10% nonoperational rate aligns with the assumption of fixed repair times in the study, where turbines undergoing significant repairs or replacements are out of service for predictable durations, contributing to the stable proportion seen in the plot.

4.2 | Risk Evaluation for Vessel Transfer and Working at Height

The blade repair process in offshore wind farms is divided into several critical phases, each with specific decision points and safety considerations. This section will address the safety considerations and modeling strategies for the case of minor crack repairs described and identified in the previous section. Figure 10 summarizes the key stages considered in the present case study.

The simulation of this repair assumes the mobilization of personnel and equipment. The assumptions made here consist of including two blade repair specialists, two rope access technicians, and two safety officers alongside the necessary equipment, such as a crew transfer vessel (CTV), ropes and harnesses, UV curing lamps, composite patch materials, and safety gear.

The port preparation phase initially involves inspection, risk assessment, and a go/no-go decision based on weather forecasts and readiness. During navigation to the site, the team continuously monitors weather conditions to ensure safe transit. Upon arrival, a safety briefing precedes the vessel transfer, where sea state and wind speed are assessed to determine whether the proceeding is safe.

Once the crew safely transfers to the wind turbine, they prepare for climbing, ensuring all safety gear is secure and the weather conditions are favorable. During the working-at-height phase, repair specialists perform the crack repair using composite patches and UV curing lamps. This phase requires continuous monitoring of weather conditions and stability.

After completing the repair, the team prepares for the descent, ensuring all safety measures are in place. The descent and subsequent vessel transfer back to the CTV are carefully executed, considering real-time weather conditions. The final phase involves navigation back to port, with continuous weather monitoring to ensure a safe return.

Throughout these phases, key factors such as weather conditions significantly influence decision-making, especially regarding vessel transfer and working at height. Safety considerations include the reliability of equipment, emergency preparedness, and risk assessment models to mitigate potential hazards.

The two most critical phases are the vessel transfer and working at height. The specific risk assessment categories can be identified in the particular phase of analysis by looking at the RAM presented in Figure 5.

Table 5 below presents a combined risk assessment for vessel transfer and working at height in offshore wind operations. It categorizes the nature of hazards, identifies the persons at risk, describes the possible effects of these hazards, and assigns a safety rating to each scenario. For vessel transfer, adverse weather, equipment failure, and poor visibility are identified as primary risks, each with significant safety implications. Similarly, hazards such as equipment failure and varying wind conditions are highlighted for working at height, with adverse weather, particularly high winds, being the most critical, associated with severe consequences such as falls and fatalities.

For vessel transfer, adverse weather (high wave-wind), equipment failure, and poor visibility are identified as key hazards, with safety ratings of $C4$ for adverse weather and poor visibility and $C3$ for equipment failure, highlighting the significant risks of capsizing, personnel injury, and navigation errors. For working at height, the risks include equipment failure, moderate wind, and high wind, with safety ratings ranging from $C3$ to

FIGURE 10 | Visual sequence representing key stages in offshore wind farm blade repair. From left to right: port preparation with a coastal dock view, navigation phase with a crew transfer vessel en route to the site, vessel transfer with CTV alongside the wind turbine, reaching the nacelle depicted by technicians approaching the turbine, and the blade repair phase showing technicians performing work at height on the turbine structure. *Source:* Shutterstock, Turbine Transfers, Ørsted, and WBUR.

*D*5, indicating the severe risk of falls and fatalities under adverse weather conditions. These ratings emphasize the critical need for stringent safety measures to protect crew and technicians during these operations.

This work will focus on a simplified application of the risk assessment framework where x represents a single variable that drives the risk score. Specifically, for the vessel transfer phase, x represents wave height. For the working at height phase, x represents the wind speed. The risk function models the increased danger of vessel transfer or working at height as wave height or wind speeds rise above a threshold x_0, with the curvature parameter η adjusting how rapidly perceived risk escalates. The function captures how these weather parameters drive and impact the safety for these two phases, reflecting higher risk perceptions as conditions worsen.

Tables 6 and 7 provide a detailed summary of the quantitative factors influencing risk perception functions for both transfer operations and working at height in offshore wind turbine maintenance. These tables categorize various safety factors into low, medium, and high-risk perception levels, such as weather conditions and PPE availability.

The threshold defining the boundary between low and medium risk perception serves as the neutral reference point, x_0. This reference point is critical for establishing baseline step functions in the risk assessment matrix and building the risk perception function. For instance, in Table 6, a wave height below 1.5 m and a wind speed below 5 m/s are considered low risk, defining the neutral points for these parameters. Similarly, in Table 7, a wind speed below 4 m/s and a wave height below 1.5 m define the low-risk threshold for working at height.

These neutral reference points allow for the creation of baseline risk perception functions, which can then be integrated into the overall risk assessment matrix. By mapping the conditions above to higher risk levels (0, 0.5, and 1) according to the RAM, these tables facilitate the systematic construction of step functions that model how risk perception escalates from low to medium and high as conditions worsen.

As shown in Figure 11, for vessel transfer, the baseline risk perception function shows minimal risk up to a wave height of 1.5 m, beyond which the risk escalates sharply. This threshold reflects industry consensus on safe operational conditions. In contrast, Agent 1's risk perception increases more gradually

TABLE 5 | Combined risk assessment for vessel transfer and working at height.

Activity	Nature of hazard	Persons at risk	Possible effects of hazard	Safety
Vessel transfer	Adverse weather (high wave-wind)	Crew, technicians	Capsizing, personnel overboard	*C*4
	Equipment failure	Crew, technicians	Injury or loss of equipment	*C*3
	Poor visibility	Crew, technicians	Navigation error, collision	*C*4
Working at height	Equipment failure	Technicians	Injury, delayed repair	*C*3
	Adverse weather (medium wind)	Technicians	Slips, falls	*C*4
	Adverse weather (high wind)	Technicians	Falls, fatality	*D*5

TABLE 6 | Summary of quantitative factors influencing risk perception function for transfer operations.

	Safety factor	Low risk perception	Medium risk perception	High risk perception
Weather conditions	Wind speed	< 5 m/s	$5\text{ m/s} \le x < 13.4\text{ m/s}$	> 13.4 m/s
	Wave height	< 1.5 m	$1.5\text{ m} \le x < 3\text{ m}$	> 3 m
	Wave period	< 6 s	$6\text{ s} \le x < 16\text{ s}$	> 16 s
	Water temperature	> 15°C	$5\text{°C} \le x < 15\text{°C}$	< 5°C
	Current	< 0.25 m/s	$0.25\text{ m/s} \le x < 0.51\text{ m/s}$	> 0.51 m/s
	Visibility	Good	Mild	Limited
	Daylight	Morning	Afternoon	Night
PPE availability	Life Jackets/PFD	> 275 N	< 275 N	
	PLB (locator beacon)	Available	Not available	
	Gloves w/good grip	Available	Not available	
	Boots (waterproof)	Available	Not available	
	Immersion suit	Available	Not available	
	Warm clothes	Available	Not available	

TABLE 7 | Summary of quantitative factors influencing risk perception function for working at height.

	Safety factor	Low risk perception	Medium risk perception	High risk perception
Weather conditions	Wind speed	< 4 m/s	4–9 m/s	> 9 m/s
	Wave height	< 1.5 m	1.5–3 m	> 3 m
	Water temperature	> 15°C	5°C–15°C	< 5°C
	Visibility	Good	Mild	Limited
PPE availability	Life jackets/PFD	Available	Not available	
	Gloves	Available	Not available	
	Immersion suit	Available	Not available	
	Safety harness	Available	Not available	

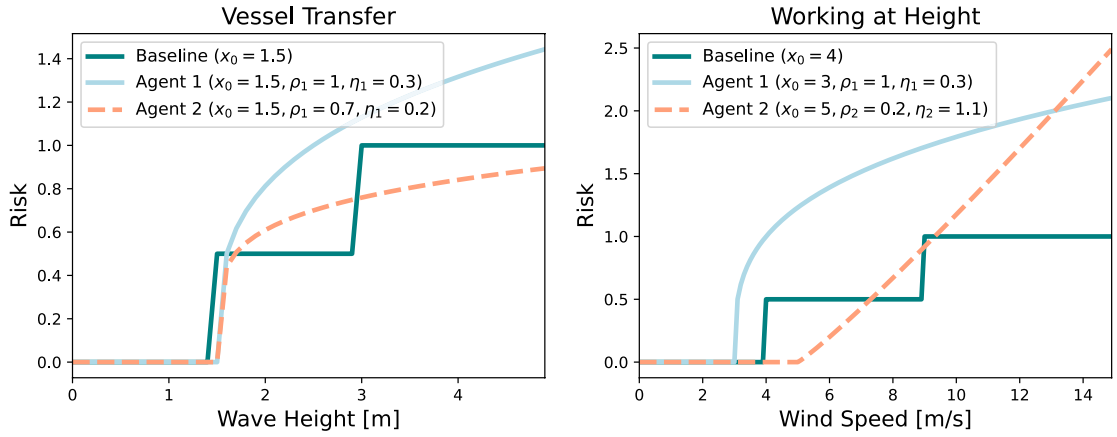

FIGURE 11 | Risk perception functions for vessel transfer and working at height, with baseline scenarios derived from neutral safety thresholds. The plots illustrate how different agents perceive risk in response to increasing wave height and wind speed, reflecting varying levels of risk aversion and sensitivity to environmental conditions.

beyond the same threshold, indicating a more cautious approach that acknowledges escalating risk in a more nuanced manner. Agent 2 perceives a slower increase in risk, suggesting a consistently higher sensitivity to wave height variations across the spectrum.

In the working-at-height scenario, the baseline risk perception function follows a similar pattern, significantly increasing perceived risk beyond the neutral point of 4 m/s wind speed. This sharp rise highlights the critical safety concern associated with higher wind speeds. Agent 1, however, begins to perceive increased risk at lower wind speeds, reflecting a lower tolerance for risk and a preference for heightened caution. Agent 2's more linear risk perception suggests a steadier approach to risk escalation, indicating confidence in managing risks even as conditions worsen.

These varying risk perceptions highlight the differences in risk tolerance among stakeholders, emphasizing the importance of incorporating such models into decision-making frameworks.

Figure 12 illustrates the simulated wind speed and wave height over a week and their corresponding impact on risk perception for different agents, aiding in determining the optimal day for intervention. The top plot combines wind speed and wave height data over the simulated period, with wind speed on the left y axis and wave height on the right y axis. The middle plot shows the risk scores associated with wave height, whereas the bottom plot displays the risk scores associated with wind speed. The baseline risk, Agent 1 (more risk averse), and Agent 2 (more risk tolerant) are compared. The variations in risk scores reflect how each agent's perception changes with the environmental conditions, highlighting the differences in decision-making strategies under fluctuating wind and wave conditions. The highest risks are observed around September 26, coinciding with peak wind speeds and wave heights. As conditions improve later in the week, the risk scores decrease, with the baseline returning to zero when conditions fall below critical thresholds. The optimal day for intervention, where risks are minimized, can be identified by the lowest risk scores later in the week, signaling safer conditions for going out.

4.3 | Combined Prospect Value Assessment

Figure 13 presents the normalized combined prospect values for two simulated agents across a series of intervention scenarios. The normalization process was employed to rescale the economic and safety prospect values to a common range, making it easier to compare the decision-making strategies

of the two agents on a qualitative level. This normalization was achieved by first subtracting the minimum value of the respective prospect functions and then dividing by the maximum value, ensuring that both the economic and safety prospects fall within a [0, 1] range. This approach allows for focusing on relative changes in prospect values rather than their absolute magnitudes, providing clearer insights into the agents' decision-making processes.

Figure 13 illustrates the normalized combined prospect values derived from integrating economic and safety considerations for two simulated agents. With a lower risk tolerance and higher sensitivity to both wave height and wind speed (see Figure 12), Agent 1 perceives relatively high safety risks even at low wind speeds. This is evident from the combined prospect value trend, where Agent 1 shows a sharp decrease only when the wind and waves drop below the tolerance threshold. This drop alleviates

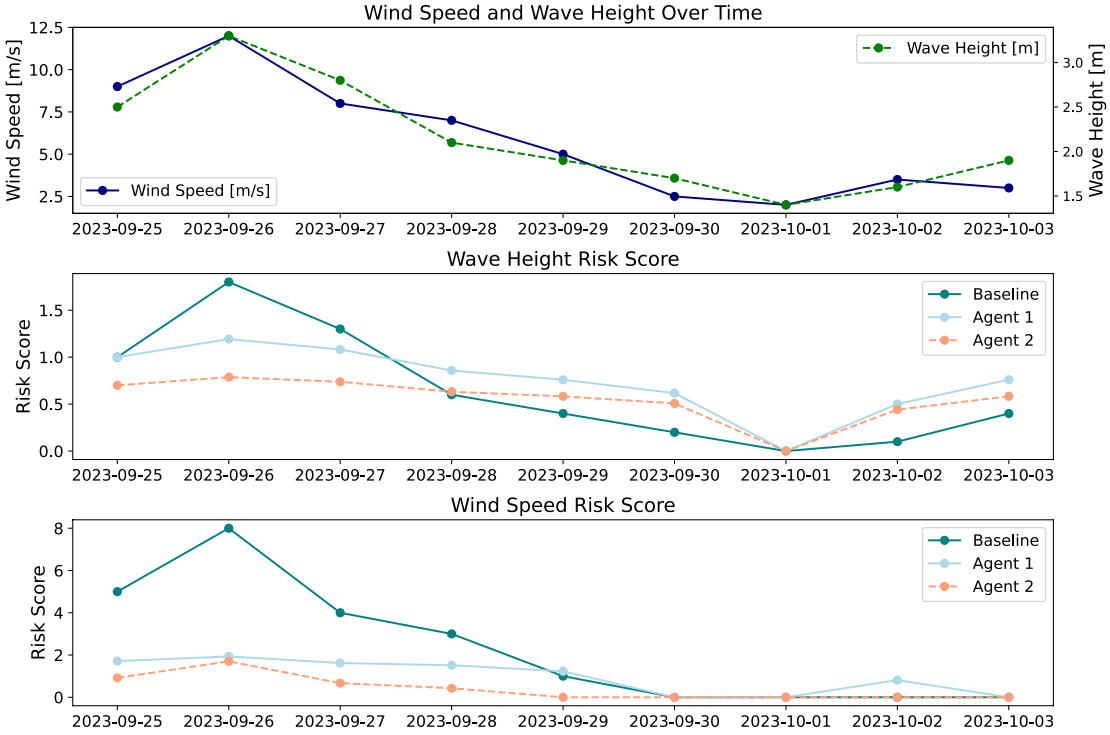

FIGURE 12 | Temporal analysis of wind speed, wave height, and corresponding risk perceptions for two simulated agents.

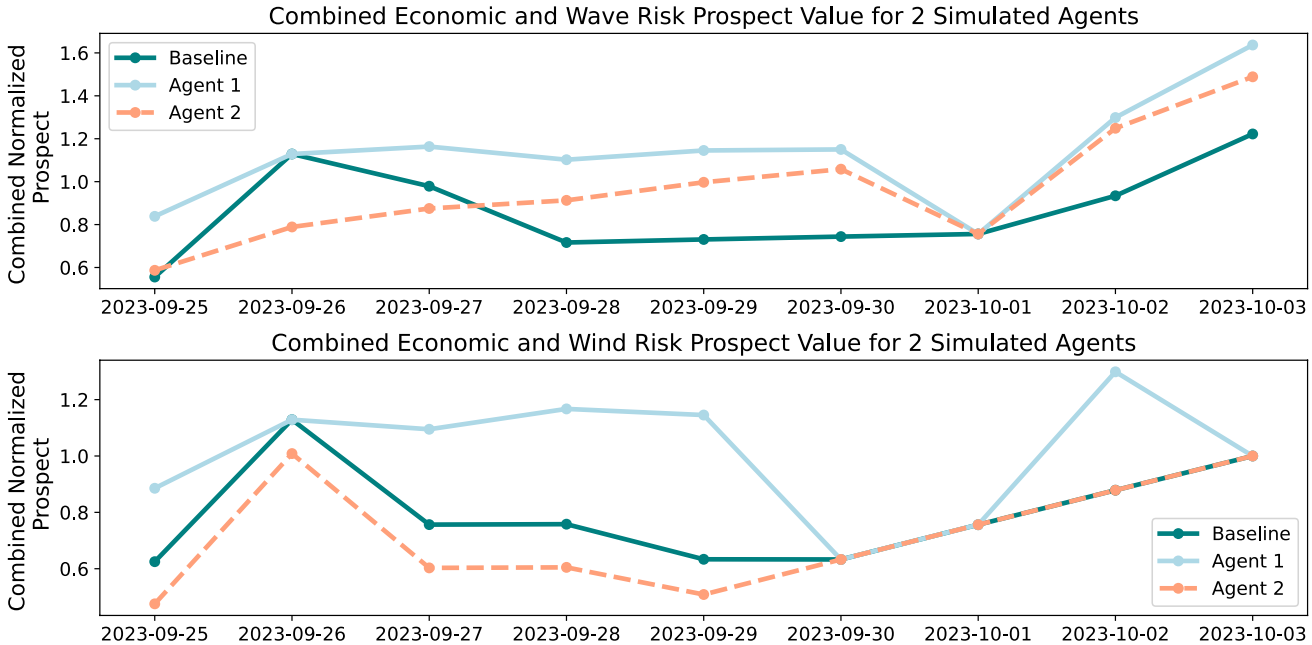

FIGURE 13 | Combined prospect values for two simulated agents over a series of intervention scenarios. The intervention index reflects different potential days or scenarios for action, highlighting the differences in decision-making strategies between the two agents relative to a raw baseline decision.

the perceived safety risk for Agent 1, leading to a significant decrease in the prospect value. This change underscores Agent 1's cautious strategy, prioritizing safety and early intervention as soon as conditions improve.

On the other hand, Agent 2, with a higher risk threshold, has lower sensitivity to both wave height and wind speeds (see Figure 12), showing a more moderate response to changes in wave and wind conditions. The prospect value for Agent 2 increases gradually, indicating a strategy that is less reactive to immediate changes in wind speed. Agent 2's higher tolerance for safety risks allows for a more immediate intervention approach, reflected in the steadier rise in the combined prospect value over time, even as wind speeds vary throughout the observed period.

Despite both agents sharing the same economic coefficient ($\gamma = 0.7$), their safety parameters drive different overall strategies. Agent 1's economic considerations are more strongly influenced by the immediate need to reduce safety risks, leading to quicker and more substantial changes in combined prospect value as soon as safer conditions (lower wind speeds) are perceived. Agent 2, however, balances economic and safety concerns differently. With a higher tolerance for wind speed risks, Agent 2 is willing to take immediate action regardless of changing conditions. This reflects a strategy that integrates economic potential more heavily over immediate safety concerns, particularly when wind speeds are high.

The wind speed peaked on September 26th, leading to the highest risk perception, especially for Agent 1. As wind speeds decreased after this peak, Agent 1's prospect value saw a sharp increase, indicating that this agent found it more advantageous to intervene quickly as soon as the risk level (due to high wind speeds) dropped. Agent 2, however, remained more conservative in their prospect value increase, reflecting a strategy of waiting for even more favorable conditions before considering intervention.

The variations in combined prospect value between the two agents highlight how different safety sensitivities and risk tolerances shape their decision-making strategies in response to environmental changes, such as wind speed. Agent 1, with a stronger emphasis on safety, responds more immediately to reductions in wind speed, leading to more dramatic changes in prospect value. In contrast, Agent 2, which is more economically driven and less sensitive to wind speed changes, shows a more gradual change in prospect value, reflecting a strategy that favors early intervention. This differentiation illustrates the flexibility and applicability of the combined prospect value model in capturing diverse decision-making approaches under varying environmental conditions.

5 | Discussion

This paper introduced a comprehensive framework for managing offshore wind turbine maintenance, designed to guide the process from initial defect detection through to optimal decision-making for intervention. The proposed strategy is versatile and can be adapted to various application domains, such as onshore wind and other industrial settings, where maintenance needs differ based on environmental and operational factors. For instance, in onshore wind maintenance, the framework could focus more on land-based logistical considerations, such as equipment availability and cost efficiency, while placing less emphasis on challenges like extreme weather and restricted accessibility that are critical offshore. Onshore applications would likely prioritize minimizing downtime and maximizing equipment availability over addressing high-stakes safety risks associated with vessel transfers or harsh marine conditions.

The framework can support flexible, real-case scenario integrated maintenance strategies, enabling, for example, a mix of condition-based and preventive approaches. Condition-based monitoring would target high-risk components, triggering maintenance only when necessary, whereas preventive schedules for less critical systems would ensure steady functionality and reduce unexpected failures. This dual approach would introduce an adjustment of the economic costs and defect assessments, stabilizing defect progression and enhancing cost efficiency. Preventive maintenance would help slow wear in less critical components, improving prediction and planning for maintenance intervals. By combining these strategies, the framework could achieve optimal reliability, cost-effectiveness, and safety across all operational areas.

Although robust, this framework has some limitations. It currently assesses risk based on a single variable, like wind speed, whereas maintenance decisions are influenced by multiple interacting factors. Future research will aim to incorporate multivariable risk assessments for a more comprehensive analysis. Additionally, the Markov model relies on assumed transition probabilities for defect progression, which may oversimplify real-world defect behavior due to limited empirical data. Refining these probabilities with real-world data is essential for improving predictive accuracy. The model's validation relies on numerical simulations, lacking the integration of real-time monitoring data, which limits its adaptability and does not fully capture the complexity of actual offshore environments. Incorporating real-time monitoring would allow for dynamic updates and more responsive decision-making. Addressing these limitations in future work will enhance the framework's accuracy and applicability in offshore wind maintenance.

Finally, although the proposed framework treats safety as a key decision factor, it remains agnostic to farm-specific standards due to limited public access to project-level implementation data, often constrained by jurisdictional and proprietary factors. As a result, the proposed framework focuses on capturing variations in safety priorities and regulatory emphasis, rather than prescribing or evaluating specific compliance pathways. Future work will aim to incorporate empirical case studies as more standardized and transparent data become available.

The framework's flexibility and robustness make it a strong candidate for further development, particularly in the context of multiscale, multistakeholder modeling. Although this study focused on a narrow application via a numerical model, future research will extend the framework to incorporate a broader range of stakeholders and temporal scales, enabling a more comprehensive analysis of offshore wind operations. This extension will provide deeper insights into the complex interactions between stakeholders, further enhancing the framework's utility in research and practical applications.

Acknowledgments

This study is partially supported by the National Science Foundation grant 2230630. The authors would like to thank Beth Rosenberg, Barbara Kates-Garnick, and Bruce Boghosian for many conversations that helped to shape this work.

Conflicts of Interest

The authors declare no conflicts of interest.

Data Availability Statement

The data that support the findings of this study are available from the corresponding author upon reasonable request.

Peer Review

The peer review history for this article is available at https://www.webofscience.com/api/gateway/wos/peer-review/10.1002/we.70065.

References

1. S. F. President and B. Sets, *Greenhouse Gas Pollution Reduction Target Aimed at Creating Good-Paying Union Jobs and Securing US Leadership on Clean Energy Technologies* (White House, 2030), 2021.

2. D. M. Frangopol and M. Liu, "Maintenance and Management of Civil Infrastructure Based on Condition, Safety, Optimization, and Life-Cycle Cost," *Structures and Infrastructure Systems* (2019): 96–108.

3. M. Li, X. Jiang, J. Carroll, and R. R. Negenborn, "A Multi-Objective Maintenance Strategy Optimization Framework for Offshore Wind Farms Considering Uncertainty," *Applied Energy* 321 (2022): 119284.

4. T. Stehly and P. Duffy, "Cost of Wind Energy Review," Tech. Rep, National Renewable Energy Lab. (NREL), Golden, CO (United States); 2020 (2021).

5. J. L. Beck, E. Chan, A. Irfanoglu, and C. Papadimitriou, "Multi-Criteria Optimal Structural Design Under Uncertainty," *Earthquake Engineering and Structural Dynamics* 28, no. 7 (1999): 741–761.

6. D. M. Frangopol, "Multicriteria Reliability-Based Structural Optimization," *Structural Safety* 3, no. 1 (1985): 23–28.

7. A. Tversky and D. Kahneman, "Advances in Prospect Theory: Cumulative Representation of Uncertainty," *Journal of Risk and Uncertainty* 5 (1992): 297–323.

8. L. Wang, Q. Liu, and T. Yin, "Decision-Making of Investment in Navigation Safety Improving Schemes With Application of Cumulative Prospect Theory," *Proceedings of the Institution of Mechanical Engineers, Part O: Journal of Risk and Reliability* 232, no. 6 (2018): 710–724.

9. Q. Liu, Y. Sun, and M. Wu, "Decision-Making Methodologies in Offshore Wind Power Investments: A Review," *Journal of Cleaner Production* 295 (2021): 126459.

10. Y. Liu, Z. P. Fan, and Y. Zhang, "Risk Decision Analysis in Emergency Response: A Method Based on Cumulative Prospect Theory," *Computers & Operations Research* 42 (2014): 75–82.

11. R. Louhichi, J. Pelletan, and M. Sallak, "Application of Prospect Theory in the Context of Predictive Maintenance Optimization Based on Risk Assessment," *Applied Sciences* 12, no. 22 (2022): 11748.

12. C. Gong, D. M. Frangopol, and M. Cheng, "Application of Cumulative Prospect Theory to Optimal Inspection Decision-Making for Ship Structures," in *Springer* (River Publishers, 2020), 65–74.

13. M. Cheng and D. M. Frangopol, "Life-Cycle Optimization of Structural Systems Based on Cumulative Prospect Theory: Effects of the Reference Point and Risk Attitudes," *Reliability Engineering & System Safety* 218 (2022): 108100.

14. J. Moubray, *Reliability-Centered Maintenance* (Industrial Press Inc, 2001).

15. J. Igba, K. Alemzadeh, C. Durugbo, and K. Henningsen, "Performance Assessment of Wind Turbine Gearboxes Using In-Service Data: Current Approaches and Future Trends," *Renewable and Sustainable Energy Reviews* 50 (2015): 144–159.

16. J. Knezevic, *Systems Maintainability. 1* (Springer Science & Business Media, 1997).

17. F. Ding and Z. Tian, "Opportunistic Maintenance for Wind Farms Considering Multi-Level Imperfect Maintenance Thresholds," *Renewable Energy* 45 (2012): 175–182.

18. Y. Lei, N. Li, S. Gontarz, J. Lin, S. Radkowski, and J. Dybala, "A Model-Based Method for Remaining Useful Life Prediction of Machinery," *IEEE Transactions on Reliability* 65, no. 3 (2016): 1314–1326.

19. C. Crabtree, Y. Feng, and P. Tavner, "Detecting Incipient Wind Turbine Gearbox Failure: A Signal Analysis Method for On-Line Condition Monitoring," 2023. 2010:154156.

20. J. Pacheco, F. Pimenta, S. Pereira, Á. Cunha, and F. Magalhães, "Fatigue Assessment of Wind Turbine Towers: Review of Processing Strategies With Illustrative Case Study," *Energies* 15, no. 13 (2022): 4782.

21. C. Bunks, D. McCarthy, and T. Al-Ani, "Condition-Based Maintenance of Machines Using Hidden Markov Models," *Mechanical Systems and Signal Processing* 14, no. 4 (2000): 597–612.

22. A. Haensch, E. M. Tronci, B. Moynihan, and B. Moaveni, "Regularized Hidden Markov Modeling With Applications to Wind Speed Predictions in Offshore Wind," *Mechanical Systems and Signal Processing* 211 (2024): 111229.

23. X. Li, D. Ouelhadj, X. Song, et al., "A Decision Support System for Strategic Maintenance Planning in Offshore Wind Farms," *Renewable Energy* 99 (2016): 784–799.

24. I. Dinwoodie, D. McMillan, M. Revie, I. Lazakis, and Y. Dalgic, "Development of a Combined Operational and Strategic Decision Support Model for Offshore Wind," *Energy Procedia* 35 (2013): 157–166.

25. M. Hofmann and I. B. Sperstad, "NOWIcob—A Tool for Reducing the Maintenance Costs of Offshore Wind Farms," *Energy Procedia* 35 (2013): 177–186.

26. A. Myhr, C. Bjerkseter, A. Ågotnes, and T. A. Nygaard, "Levelised Cost of Energy for Offshore Floating Wind Turbines in a Life Cycle Perspective," *Renewable Energy* 66 (2014): 714–728.

27. L. Dai, M. Rausand, and I. B. Utne, "Availability Centred Maintenance for Offshore Wind Farms," *Journal of Quality in Maintenance Engineering* 21, no. 4 (2015): 403–418.

28. J. McMorland, M. Collu, D. McMillan, J. Carroll, and A. Coraddu, "Opportunistic Maintenance for Offshore Wind: A Review and Proposal of Future Framework," *Renewable and Sustainable Energy Reviews* 184 (2023): 113571.

29. J. D. Sørensen, "Framework for Risk-Based Planning of Operation and Maintenance for Offshore Wind Turbines," *Wind Energy: An International Journal for Progress and Applications in Wind Power Conversion Technology* 12, no. 5 (2009): 493–506.

30. C. D. Lai, D. Murthy, and M. Xie, *Weibull Distributions and Their Applications* (Springer, 2006), 63–78.

31. J. Carroll, A. McDonald, and D. McMillan, "Failure Rate, Repair Time and Unscheduled O&M Cost Analysis of Offshore Wind Turbines," *Wind Energy* 19, no. 6 (2016): 1107–1119, https://doi.org/10.1002/we.1887.

32. C. Dao, B. Kazemtabrizi, and C. Crabtree, "Wind Turbine Reliability Data Review and Impacts on Levelised Cost of Energy," *Wind Energy* 22, no. 12 (2019): 1848–1871.

33. GH R, "Reliability Focused Research on Optimizing Wind Energy Systems Design, Operation and Maintenance: Tools, Proof of Concepts, Guidelines & Methodologies for a New Generation," Reliawind, Rep. (2007).

34. L. Mishnaevsky, Jr. and K. Thomsen, "Costs of Repair of Wind Turbine Blades: Influence of Technology Aspects," *Wind Energy* 23, no. 12 (2020): 2247–2255.

35. BVG Associates, "Guide to a Floating Offshore Wind," (2023), https://guidetofloatingoffshorewind.com/guide/i-installation-and-commissioning/i-5-floating-offshore-wind-turbine-assembly/i-5-1-heavy-lifting-and-moving-equipment/.

36. US Department of Labor, *Occupational Outlook Handbook, Wind Turbine Technicians* (Bureau of Labor Statistics, 2000), https://www.bls.gov/ooh/installation-maintenance-and-repair/wind-turbine-technicians.htm.

37. S. Faulstich, B. Hahn, and P. J. Tavner, "Wind Turbine Downtime and Its Importance for Offshore Deployment," *Wind Energy* 14, no. 3 (2011): 327–337.

38. R. H. Wiser and M. Bolinger, "Laboratory LBN. 2018 Wind Technologies Market Report," (2019), https://www.energy.gov/sites/prod/files/2019/08/f65/2018%20Wind%20Technologies%20Market%20Report%20FINAL.pdf.

39. P. Ellwood, J. Reynolds, and M. Duckworth, *Green Jobs and Occupational Safety and Health: Foresight on New and Emerging Risks Associated With New Technologies by 2020* (European Agency for Safety and Health at Work, 2014).

40. D. Rowell, D. McMillan, and J. Carroll, "Offshore Wind H&S: A Review and Analysis," *Renewable and Sustainable Energy Reviews* 189 (2024): 113928.

41. J. Fraser and J. Stewart, "Worker Safety in Offshore Wind," Presented at NYSERDA Webinar Series, (2023), Retrieved from https://www.nyserda.ny.gov/osw-webinar-series.

42. Bureau of Ocean Energy Management and and Bureau of Safety and Environmental Enforcement, "Code of Federal Regulations, Title 30: Mineral Resources," Sections 585–586 (BOEM) and 285 (BSEE), (2024), https://www.ecfr.gov/current/title-30.

43. Bureau of Ocean Energy Management and and Bureau of Safety and Environmental Enforcement, "Code of Federal Regulations, Title 30: Mineral Resources, Part 285," (2024), https://www.ecfr.gov/current/title-30/chapter-II/subchapter-B/part-285.

44. K. Sligh and E. Klein, "BSEE/BOEM Renewable Energy Split Rule Information and Q&a: AA003 Reorganization of Title 30—Renewable Energy and Alternate Uses of Existing Facilities on the Outer Continental Shelf," Presented at BSEE/BOEM Split Rule Workshop, (2023).

45. Occupational Safety and Health Administration, "Occupational Safety and Health Administration Standards," (2024), https://www.osha.gov.

46. WINDExchange, "Offshore Wind Workforce Safety Standards and Training Resource," (2024), https://windexchange.energy.gov.

47. Wind Organisation Global, "Training Standards for a Safer and More Productive Workforce," (2024), https://www.globalwindsafety.org.

48. G+ Global Offshore Wind Health and Safety Organisation, "Annual Report," accessed: 2024-MM-DD, https://www.gplusoffshorewind.com/publications/annual-reports.

49. International Marine Contractors Association (IMCA), "Guidance and Best Practices," accessed 2024-MM-DD, https://www.imca-int.com/publications/guidance/.

50. K. Gao, L. Sun, Y. Yang, F. Meng, and X. Qu, "Cumulative Prospect Theory Coupled With Multi-Attribute Decision Making for Modeling Travel Behavior," *Transportation Research Part A: Policy and Practice* 148 (2021): 1–21.

51. Y. Yu, S. Wu, J. Yu, Y. Xu, L. Song, and W. Xu, "A Hybrid Multi-Criteria Decision-Making Framework for Offshore Wind Turbine Selection: A Case Study in China," *Applied Energy* 328 (2022): 120173.

52. M. Allais, "Le Comportement de l'Homme Rationnel Devant le Risque: Critique des Postulats et Axiomes de l'École Américaine," *Econometrica: Journal of the Econometric Society* 21 (1953): 503–546.

53. D. Prelec, "The Probability Weighting Function," *Econometrica* 66 (1998): 497–527.

54. D. A. Hensher, W. H. Greene, and Z. Li, "Embedding Risk Attitude and Decision Weights in Non-Linear Logit to Accommodate Time Variability in the Value of Expected Travel Time Savings," *Transportation Research Part B: Methodological* 45, no. 7 (2011): 954–972.

55. M. Razo and S. Gao, "A Rank-Dependent Expected Utility Model for Strategic Route Choice With Stated Preference Data," *Transportation Research Part C: Emerging Technologies* 27 (2013): 117–130.

56. H. P. Stott, "Cumulative Prospect Theory's Functional Menagerie," *Journal of Risk and Uncertainty* 32 (2006): 101–130.

57. M. A. Boyd and S. Lau, "An Introduction to Markov Modeling: Concepts and Uses," (1998).

58. C. I. Ossai, B. Boswell, and I. J. Davies, "A Markovian Approach for Modelling the Effects of Maintenance on Downtime and Failure Risk of Wind Turbine Components," *Renewable Energy* 96 (2016): 775–783.

59. S. Adumene and A. Okoro, "A Markovian Reliability Approach for Offshore Wind Energy System Analysis in Harsh Environments," *Engineering Reports* 2, no. 3 (2020): e12128.

60. B. Vandeskog, "Risk, Trust and Reputation in the Norwegian Offshore Supply Chain," *Safety Science* 163 (2023): 106118.

61. Risk DMU, "The Neural Basis of Loss Aversion in Science," (2007); 1134239(515):315.

62. K. Kong, K. Dyer, C. Payne, I. Hamerton, and P. M. Weaver, "Progress and Trends in Damage Detection Methods, Maintenance, and Data-Driven Monitoring of Wind Turbine Blades—A Review," *Renewable Energy Focus* 44 (2023): 390–412.

63. L. Mishnaevsky, Jr., "Root Causes and Mechanisms of Failure of Wind Turbine Blades: Overview," *Materials* 15, no. 9 (2022): 2959.

64. M. Ge, H. Zhang, Y. Wu, and Y. Li, "Effects of Leading Edge Defects on Aerodynamic Performance of the S809 Airfoil," *Energy Conversion and Management* 195 (2019): 466–479.

65. Ö. S. Özçakmak, D. Bretos, B. Méndez, and C. Bak, *Determination of annual energy production loss due to erosion on wind turbine blades* (IOP Publishing, 2024).

66. L. Mishnaevsky, Jr., "Toolbox for Optimizing Anti-Erosion Protective Coatings of Wind Turbine Blades: Overview of Mechanisms and Technical Solutions," *Wind Energy* 22, no. 11 (2019): 1636–1653.

67. L. Mishnaevsky, Jr., "Repair of Wind Turbine Blades: Review of Methods and Related Computational Mechanics Problems," *Renewable Energy* 140 (2019): 828–839.

68. J. Yang, C. Peng, J. Xiao, et al., "Structural Investigation of Composite Wind Turbine Blade Considering Structural Collapse in Full-Scale Static Tests," *Composite Structures* 97 (2013): 15–29.

69. T. Harrell, O. Thomsen, and J. M. Dulieu-Barton, "Predicting the Effect of Lightning Strike Damage on the Structural Response of CFRP Wind Blade Sparcap Laminates," *Composite Structures* 308 (2023): 116707.

70. E. Lantz, *Operations Expenditures: Historical Trends and Continuing Challenges* (National Renewable Energy Laboratory, 2013).